Characterization of a soluble anthradithiophene derivative

B. R. Conrad,[1,a)] C. K. Chan,[1,b)] M. A. Loth,[2] S. R. Parkin,[2] X. Zhang,[1] D. M. DeLongchamp,[1] J. E. Anthony,[2] and D. J. Gundlach[1]
[1]*National Institute of Standards and Technology, Gaithersburg, Maryland 20899, USA*
[2]*Department of Chemistry, University of Kentucky, Lexington, Kentucky 40506, USA*

(Received 18 July 2010; accepted 4 September 2010; published online 1 October 2010)

The structural and electrical properties of a solution processable material, 2,8-difluoro-5,11-tert-butyldimethylsilylethynyl anthradithiophene (TBDMS), were measured for single crystal transistors. TBDMS is observed to readily form single crystals from physical vapor zone sublimation. A columnar packing crystal structure, with an approximate $\pi/4$ radian rotational offset between neighboring molecules, is observed. Single crystal TBDMS transistors display a maximum observed saturation mobility μ_S of 0.07 $cm^2/V\,s$, current on-off ratio $>10^7$, and subthreshold swing $S \approx 1$ dec/V. The spectral current noises of single crystal devices display a $1/f$ flicker noise, while the metal-semiconductor charge injection barrier is estimated by ultraviolet photoemission spectroscopy. © *2010 American Institute of Physics*. [doi:10.1063/1.3495998]

Organic semiconductors continue to be an active research area since opportunities to tailor their physical and electrical properties can be exploited to fabricate commercial devices by low-cost, solution-based processing methods. Several high-mobility oligomers, such as pentacene and rubrene,[1] have been identified; yet, many are incompatible with rapid manufacturing methods because of poor solubility or film structure.[2–4] Chemical modification of high performance molecules is a typical approach to tailor solubility, charge mobility, frontier states, and film microstructure. Side group additions and direct atom substitution are among the common modification methods.[5–7] Such recently developed organic semiconducting materials are among the forefront of advances in the field.[8–10] Exploring the crystallographic and electronic changes induced by chemical modification is vital to continued development.

Of particular interest are organic molecules derived from a historically interesting semiconductor anthradithiophene (ADT).[11,12] It has been shown that chemical modification can dramatically change thin-film formation,[13] bulk structures,[9] and device performance.[12] These relationships must be understood at least phenomenologically since the commercial applications for organic materials require a myriad of operating conditions and processing schemes.[2] In this paper, the ADT derivative 2,8-difluoro-5,11-(bis(tert-butyldimethylsilylethynyl)) anthradithiophene (TBDMS) [Fig. 2(b) inset] is characterized in the single crystal and thin-film transistor (TFT) configuration. The material was synthesized as described elsewhere,[14] only substituting tert-butyldimethylsilyl acetylene for triethylsilyl acetylene. TBDMS crystals adopt a columnar packing structure with an approximate $\pi/4$ radian ($\approx 45°$) rotational offset between neighboring molecules in the stack by x-ray diffraction (XRD) and electron diffraction (ED). The performance of single crystal TFTs is compared to that of spun coat devices while the effects of a contact surface treatment, pentafluorobenzenethiol (PFBT), are explored. To evaluate charge injection and its impact on transport in single crystals, the metal-semiconductor interfacial barrier for PFBT treated contacts is estimated by ultraviolet photoemission spectroscopy (UPS) measurements.

All electrical test structures are bottom contact field-effect transistors. Source and drain contacts were prepatterned on Si(100) with a ≈300 nm thermal oxide by photolithography and a lift-off process. The contacts (40 nm Au on 5 nm Ti) are E-beam deposited a ≈0.1 nm/s rate. Indicated device contacts were PFBT pretreated using solution-based methods.[13,15] Single crystal transistors were fabricated to access the intrinsic electronic properties and probe the effects of highly defined molecular ordering. Thin lamellar-like crystals (XRD and ED characterized) are grown through physical vapor zone sublimation[9] at atmospheric pressures where TBDMS readily sublimes at ≈260 °C. Freshly grown crystals are then laminated on prefabricated transistor structures.[2,16] All electrical characterization was conducted in a dark nitrogen-purged probe station following an hour purging period to minimize atmospheric doping.

To relate single crystal device performance to commercially relevant solution processing methods, TFTs were fabricated on identical substrates. TBDMS dissolved in chlorobenzene at 1.0% by weight was spun on substrates with bare- and PFBT-treated contacts at 1000 rpm for 1 min in Ar. TBDMS forms an optically amorphous film with polycrystalline regions near dewetting locations and does not display the contact-induced crystallization demonstrated by other ADT derivatives for these conditions.[6] Yet, contact-induced crystallinity can occur from techniques such as drop casting. The current-voltage characteristics of a typical TBDMS-TFT are shown in Fig. 1. The left and right axes illustrate the square root of the drain current, $\sqrt{I_D}$, and the drain current, I_D, respectively, versus the gate-source voltage V_{GS} at a drain-source voltage $V_{DS}=-60$ V. For this specific device (optically measured channel length and width ratio L/W =95/76), the saturation mobility is ≈0.03 $cm^2\,V^{-1}\,s^{-1}$, threshold voltage is $V_{TH} \approx 5$ V, and on/off current ratio $I_{on}/I_{off} \approx 10^6$. The drain current I_D versus the drain-source voltage V_{DS} is the inset of Fig. 1. For the laminated crystal device, the fast crystal growth axis (001) is aligned with the

[a)]Now at Department of Physics and Astronomy, Appalachian State University, Boone, North Carolina, USA. Electronic mail: conradbr@appstate.edu.
[b)]Now at Sandia National Laboratory, Albuquerque, New Mexico, USA.

 © 2010 American Institute of Physics

Downloaded 07 Aug 2011 to 128.163.237.223. Redistribution subject to AIP license or copyright; see http://apl.aip.org/about/rights_and_permissions

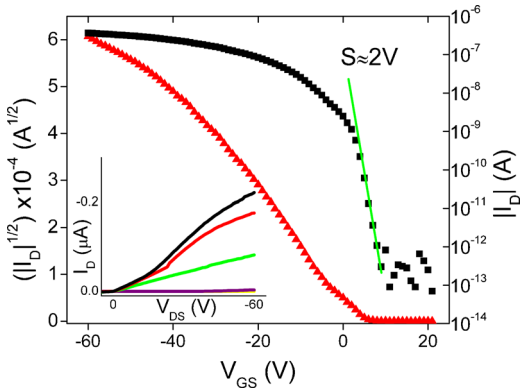

FIG. 1. (Color online) Left axis: square root of the drain current I_D magnitude vs the gate-source voltage V_{GS} at a drain-source voltage V_{DS}=−60 V for a single crystal TFT. Right axis: the magnitude of the drain current I_D vs the gate voltage V_{GS}. Inset: the drain current I_D vs the drain-source voltage V_{DS} is plotted at different gate voltages V_{GS} (Top curve: V_{GS}=−60 V, Second curve: V_{GS}=−40 V, Third curve: V_{GS}=−20 V, Bottom curve: V_{GS} =0 V).

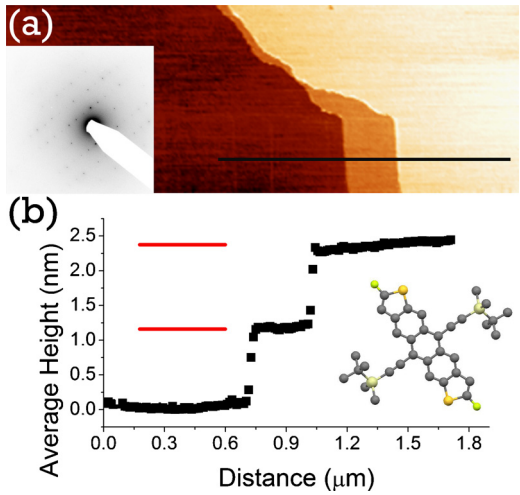

FIG. 2. (Color online) (a) AFM image (3 μm×1.5 μm) of the two steps on the surface of a TBDMS crystal. A black line indicates where the step averaging occurs to form an average height profile. Inset: ED pattern of a TBDMS single crystal at normal beam incidence. (b) This line profile is the average of 37 individual line scans. The red lines highlight the difference in height between individual steps (≈1.2 nm for this image). Inset: the molecular structure of TBDMS. (c) Illustration of TBDMS molecular order along *a* axis.

device channel to be parallel to the longitudinal field, suggesting electrical measurements in the preferred charge transport direction. The crystal has a nominal thickness of ≈400 nm, as measured by atomic force microscopy (AFM). Single crystal transistors with PFBT treated contacts display improved performance with a saturation mobility of 0.07 $cm^2\ V^{-1}\ s^{-1}$, threshold voltage $V_{TH}\sim 10$ V, and on/off current ratio I_{on}/I_{off} of $\approx 10^7$. Despite PFBT use, nonlinearities often attributed to contact effects are observed.

A summary of the spin-cast and crystalline transistor performance metrics for test structures with bare- and PFBT-treated contacts are shown in Table I. All averaged results use at least eight individual devices. For both single crystal and spun cast devices, use of a gate dielectric surface treatment, such as the self-assembled monolayer octyltrichlorosilane, modestly increased device performance but resulted in increased dewetting for spin-cast devices and increased crystal delamination.

Crystalline devices surfaces were characterized by AFM [Fig. 2(a)]. Surfaces were observed to be smooth over several square micrometers (rms <0.5 nm), molecular layers span several 100 μm, and the average molecular layer height was extracted from individual line scans [Fig. 2(b)] and measured to be 1.2 ±0.1 nm. Material grown by physical vapor transport was characterized by ED, as shown in the ED pattern of a TBDMS crystal at normal incidence [Fig. 2(a) inset]. This pattern confirms the single crystalline nature and agrees with the XRD structure of solution grown single crystals: monoclinic symmetry [a=7.9211(2) Å, b=15.3716(3) Å, c=26.6849(6) Å, β=97.0410(10)°] with an R factor of 0.1082. Figure 2(c) displays packing along the fast growth direction (001), a, with a planar backbones spacing of 0.35 nm and a columnar packing motif, with a ≈45° rotational offset between neighboring molecules [Fig. 2(c)]. This results in significantly less intermolecular aromatic overlap than seen in related materials.[12] Both ED and XRD confirm AFM measurements, proving terrace step-heights (100) of ≈1.2 nm and $\pi-\pi$ packing in the long crystal axis direction (001).

Single crystal device noise was studied to further characterize mechanisms affecting charge transport. Organic TFTs display flicker noise[13,17,18] over several decades (1 Hz to >1 kHz)[19] in linear I-V operation, consistent with established techniques.[18] The current noise spectrum is expected to have the empirical form $S_I=AI_D^2/f^\alpha$, where S is the spectral noise density, A is the noise coefficient, I_D is the drain current, f is frequency, and α is the constant frequency exponent. Figure 3 shows the normalized spectral noise density S for a typical single crystal device over several frequency decades at constant drain-source and gate-source voltage (V_{DS}=−1.0 V, V_{GS}=−20.0 V). For high performing devices, the spectral noise density S was observed to be of the form $S\propto I^{2.0\pm0.2}/f^{1.0\pm0.1}$ where the indicated uncertainties are standard deviations (2σ). Over the range where devices displayed the characteristic $A\propto 1/(V_{GS}-V_{TH})$ behavior typical of mobility fluctuations, the coefficient A is proportional to Hooge's parameter.[19] Hooge's parameter for two devices is 200 and 500, which in comparison to a related ADT deriva-

TABLE I. Performance metrics (maximum saturation mobility μ, average saturation mobility μ_{avg}, subthreshold swing S, range of threshold voltage V_{TH}, and the maximum measured on/off current ratio I_{on}/I_{off}) obtained from spin-cast and single crystal TBDMS field effect transistors. A minimum of eight devices are averaged for each measurement and uncertainties are the standard deviation.

Deposition method	Surface treatment	μ (cm^2/V s)	μ_{avg} (cm^2/V s)	S (V/dec)	V_{TH} (V)	I_{on}/I_{off}
Spin	Untreated	2×10^{-3}	5×10^{-4}	1.6 ± 0.5	−10 ± 15	10^6
Spin	PBFT	6×10^{-3}	1×10^{-3}	3.7 ± 1.6	−15 ± 10	10^6
Single crystal	Untreated	2×10^{-2}	7×10^{-3}	2.0 ± 1.3	−05 ± 10	10^7
Single crystal	PFBT	7×10^{-2}	2×10^{-2}	3.1 ± 1.9	−10 ± 15	10^8

Downloaded 07 Aug 2011 to 128.163.237.223. Redistribution subject to AIP license or copyright; see http://apl.aip.org/about/rights_and_permissions

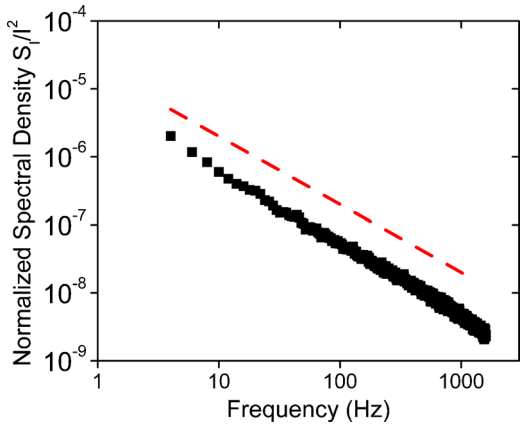

FIG. 3. (Color online) Spectral noise density S for a typical single crystal TBDMS transistor ($V_{DS}=-1.0$ V, $V_{GS}=-20.0$ V). The solid black squares can be fit to $S \propto f^{-1.01}$ in this case. The dashed line shows a $S \propto f^{-1}$ behavior to guide the eye.

tive is at least a factor of 100 larger.[13] Hooge's parameter measurements are more insightful for device comparisons while distinguishing between specific noise generation mechanisms, such as contact and conduction channel origins, is often difficult and inconclusive. However, possible explanations of the excess noise include a relatively lower mobility,[13] relatively larger XRD structural disorder (R factor), contact effects, charge trapping at the interfaces, and crystal defects.[17]

The best performing devices for this study utilized PFBT contact treated substrates,[20] yet displayed increased nonlinearities at low drain-source voltages (Fig. 1 inset). To probe this observation, Fig. 4(a) provides UPS spectra for the vacuum level onset (14–18 eV binding energy) and filled valence states (0–10 eV binding energy) of Au, PFBT treated Au, TBDMS spin-coated Au, and TBDMS spin-coated PFBT treated Au. The measured TBDMS spun-cast films are polycrystalline with areas of dewetting and display a thickness up to 200 nm. Figure 4(b) shows the energy-level structures of the metal-organic and metal-self-assembled monolayer-organic interfaces, which are averaged over the specimen in an ~5 mm^2 area. Assuming flat energy levels near the substrate, which is expected for small molecules deposited on surfaces contaminated by adventitious carbon or solution processing,[21] the average charge injection barrier for TB-

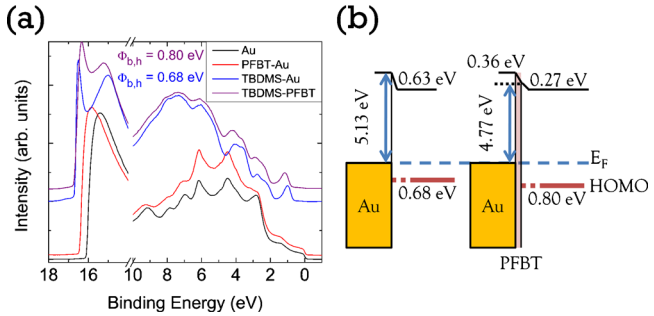

FIG. 4. (Color online) (a) UPS spectra of the vacuum level onset (left) and filled valence states (right) of Au, PFBT treated Au, TBDMS covered Au, and TBDMS covered PFBT treated Au. (b) Energy-level diagram of bare Au and PFBT treated Au comparing measured work function energies (5.13 eV and 4.77 eV respectively), shift in vacuum level for PFBT treated Au (0.36 eV), shift in vacuum levels for TBDMS covered Au/TBDMS treated Au (0.63 eV and 0.27 eV respectively), and the relative positions of HOMO level (0.68 eV and 0.80 eV below the Fermi level).

DMS spin-coated onto PFBT treated Au is observed to occur at a higher energy than the TBDMS spin-coated on bare Au [$\Phi_{b,h}$(PFBT)=0.80 eV > $\Phi_{b,h}$(bare)=0.68 eV]. Assuming that this energy level shift at spin-coated (multifaceted) TBDMS contact is similar to that of the single-crystal, this small shift of ≈0.12 eV, could generate the increased low voltage nonlinearities that are often attributed to contact effects.[1,22]

In conclusion, a soluble organic semiconductor has been electrically measured and physically characterized. In sharp contrast with related organic derivatives that typically form one-dimensional "slipstack" or two-dimensional "brickwork" stacking motifs,[23] a columnar-stacking crystal structure with a substantial rotational offset is observed. Despite the limited $\pi-\pi$ overlap between molecules and relatively high current noise, a relatively high maximum mobility of 0.07 and 0.006 cm^2/V s are observed in single crystal and spun-cast devices. UPS measurements suggest that the charge injection barrier of PFBT treated Au contacts could be correlated with poor charge injection at the metal-semiconductor interface.

NIST/NRC Postdoctoral Associateship for B.R.C. and C.K.C., the Office of Naval Research Grant No. N00014-05-1-0019 for J.E.A. and M.A.L, and C. Snyder, K. Pernstich, and O. Jurchescu for insightful discussions.

[1] O. Jurchescu, J. Baas, and T. Palstra, Appl. Phys. Lett. **84**, 3061 (2004).
[2] D. J. Gundlach, Nature Mater. **6**, 173 (2007).
[3] V. Podzorov, E. Menard, A. Borissov, V. Kiryukhin, J. Rogers, and M. Gershenson, Phys. Rev. Lett. **93**, 086602 (2004).
[4] O. D. Jurchescu, S. Subramanian, R. J. Kline, S. D. Hudson, J. E. Anthony, T. N. Jackson, and D. J. Gundlach, Chem. Mater. **20**, 6733 (2008).
[5] G. Yu, J. Gao, J. C. Hummelen, F. Wudl, and A. J. Heeger, Science **270**, 1789 (1995).
[6] D. J. Gundlach, J. E. Royer, S. K. Park, S. Subramanian, O. D. Jurchescu, B. H. Hamadani, A. J. Moad, R. J. Kline, L. C. Teague, O. Kirillov, C. A. Richter, J. G. Kushmerick, L. J. Richter, S. R. Parkin, T. N. Jackson, and J. E. Anthony, Nature Mater. **7**, 216 (2008).
[7] G. Horowitz, Adv. Mater. **10**, 365 (1998).
[8] S. S. Lee, C. S. Kim, E. D. Gomez, B. Purushothaman, M. F. Toney, C. Wang, A. Hexemer, J. E. Anthony, and Y. Loo, Adv. Mater. **21**, 3605 (2009).
[9] O. D. Jurchescu, D. A. Mourey, S. Subramanian, S. R. Parkin, B. M. Vogel, J. E. Anthony, T. N. Jackson, and D. J. Gundlach, Phys. Rev. B **80**, 085201 (2009).
[10] R. C. I. MacKenzie, J. M. Frost, and J. Nelson, J. Chem. Phys. **132**, 064904 (2010).
[11] J. G. Laquindanum, H. E. Katz, and A. J. Lovinger, J. Am. Chem. Soc. **120**, 664 (1998).
[12] J. E. Anthony, Chem. Rev. **106**, 5028 (2006).
[13] O. D. Jurchescu, B. H. Hamadani, H. D. Xiong, S. K. Park, S. Subramanian, N. M. Zimmerman, J. E. Anthony, T. N. Jackson, and D. J. Gundlach, Appl. Phys. Lett. **92**, 132103 (2008).
[14] S. Subramanian, S. K. Park, S. R. Parkin, V. Podzorov, T. N. Jackson, and J. E. Anthony, J. Am. Chem. Soc. **130**, 2706 (2008).
[15] R. J. Kline, D. M. DeLongchamp, D. A. Fischer, E. K. Lin, M. Heeney, I. McCulloch, and M. F. Toney, Appl. Phys. Lett. **90**, 062117 (2007).
[16] R. W. I. de Boer, T. M. Klapwijk, and A. F. Morpurgo, Appl. Phys. Lett. **83**, 4345 (2003).
[17] B. R. Conrad, W. G. Cullen, W. Yan, and E. D. Williams, Appl. Phys. Lett. **91**, 242110 (2007).
[18] L. K. J. Vandamme, R. Feyaerts, G. Trefán, and C. Detcheverry, J. Appl. Phys. **91**, 719 (2002).
[19] F. N. Hooge, IEEE Trans. Electron Devices **41**, 1926 (1994).
[20] C. Kuo, M. M. Payne, J. E. Anthony, and T. N. Jackson, Tech. Dig. - Int. Electron Devices Meet. **2004**, 373.
[21] A. Wan, J. Hwang, F. Amy, and A. Kahn, Org. Electron. **6**, 47 (2005).
[22] H. Sirringhaus, Adv. Mater. **17**, 2411 (2005).
[23] J. Chen, S. Subramanian, S. R. Parkin, M. Siegler, K. Gallup, C. Haughn, D. C. Martin, and J. E. Anthony, J. Mater. Chem. **18**, 1961 (2008).

Downloaded 07 Aug 2011 to 128.163.237.223. Redistribution subject to AIP license or copyright; see http://apl.aip.org/about/rights_and_permissions